ISSN (Print) 1226-1750
ISSN (Online) 2233-6656
Journal of Magnetics 23(3), 423-435 (2018) https://doi.org/10.4283/JMAG.2018.23.3.423

Modeling and Simulation of the Magnetic Method for High Voltage Direct Current Inspection Robot

Xian-jin Xu[1], Cheng-hui Liu[1]*, Yu Yan[2], Hao-da Chen[1], Lei Fang[3], Yun-long Wang[1], and Long-hui Wu[1]

[1]*College of Mechanical Engineering, Hubei University of Technology, Wuhan, Hubei Province, China*
[2]*State Grid of Human Electric Power Company, Changsha, Hunan Province, China*
[3]*Wuhan Heyue Equipment Technol. Co. Ltd, Wuhan, Hubei Province, China*

(Received 26 January 2018, Received in final form 27 July 2018, Accepted 1 August 2018)

In order to solve the slipping problem of a two-arm-wheel combined inspection robot, a maglev system based on the magnetic field of a high voltage direct current (HVDC) is proposed. The magnetic system comprises of two parts: a magnetic levitation system and a magnetic drive system. The levitation component overcomes the gravity of the robot by the Ampere force generated by current-carrying coils in the magnetic field of HVDC. The drive component utilizes the Ampere force generated by current-carrying coils in the magnetic field of HVDC as the driving force. Simulation results of the model are compared with the calculated values. The results show that the magnetic levitation method and the magnetic drive method are theoretically feasible, and the model is accurate and effective, which is of great practical significance to the physical realization of the inspection robot.

Keywords : ampere force, HVDC, inspection robot, magnetic system, modeling, simulation

1. Introduction

Since the late 1980s, the use of mobile robots for overhead high-voltage circuit inspection has become a hot topic in the field of robotics [1-3]. Canada's Quebec Hydro, KEPCO and JPS are notable examples of high-voltage circuit inspection robots. The Canada's Quebec Hydro developed a “LineScout” inspection robot [4, 5]. The KEPCO developed a multi-split wire patrol robot called “Expliner” [6]. The Wuhan University research team has developed a multi-split line of two independent inspection robot prototypes to adapt to 220 kV single split line and 220-550 kV [7-9]. Although research on high-voltage inspection line robots have made great progress, there is still a great gap to overcome in terms of the degree of practicality. A more prominent technical challenge involves the traveling wheel slip. Most of the high-voltage inspection robots use a wheel-armed structure, and the static friction force traction robot moves between the driving wheel and the surface of the line. When the surface of the line is unpredictable (such as icing), the static friction is not enough to overcome the gravity, which results in slipping. A slip seriously affects the robot inspection efficiency, increases the energy burden of the robot, and may cause damage to the transmission line. When the slip is serious, the robot becomes difficult to control. Slip is the inherent problem of wheel drive and changing the traction of the robot can eliminate the slip problem.

The technology applied in magnetic levitation trains [10-12] and linear motors [13, 14] provides a new way to solve the problems such as slipping of inspection robot. The magnetic levitation method and magnetic drive method described in this paper are different from the maglev train technology. The magnetic principle states that same poles repel each other and the opposite poles attract each other, which lays the foundation of the levitation of the train. However, by the use of HVDC transmission lines around the magnetic field and appropriate arrangement of coils, magnetic levitation can overcome the robot's own gravity by exploiting the Ampere force generated by current-carrying coil in the magnetic field. The magnetic drive harnesses the Ampere force generated by current-carrying coils in the magnetic

*Corresponding author: Tel: +86-15926411039
Fax: +86-15926411039, e-mail: 15926411039@163.com

field as the driving force of the traction robot to replace the wheel drive mode, thus solving the slipping problem of inspection robots.

2. Design of the Overall Structure of Inspection Robot

Research into high-pressure inspection robots has mostly focused on the wheel-armed structure so far. These types of inspection robots are large, bulky, inefficient, and have poor resistance to wind load and other defects. In order to realize magnetic levitation and magnetic drive, the proposed inspection robot is designed in an intermediate cylindrical shape with curved ends (to reduce the air resistance during operation). The overall structure of inspection line robot is designed as shown in Fig. 1. The robotic magnetic levitation system includes magnetic suspension system and magnetic drive system. The magnetic levitation system and the magnetic drive system are joined together, since the use of magnetic drive system cascade can increase the driving force.

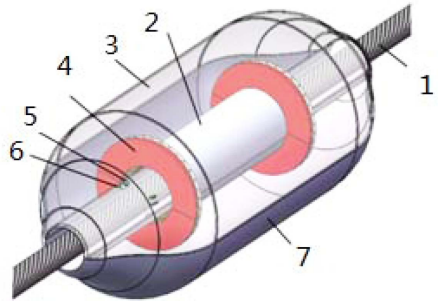

1-High-voltage lines; 2-Magnetic levitation system; 3-Upper body; 4-Magnetic drive system; 5-Small roller holder; 6-Small roller; 7-Lower body

Fig. 1. (Color online) Overall Structure of the Magnetic Inspection Robot.

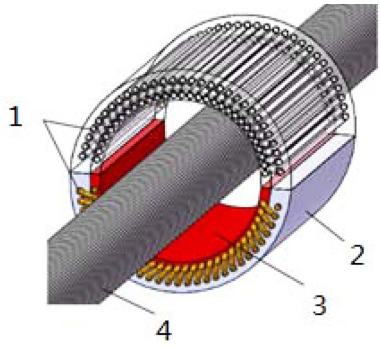

1-Current-carrying coils; 2-Hard magnetic material; 3-Soft magnetic material; 4-High-voltage lines

Fig. 2. (Color online) Entity model of magnetic levitation system.

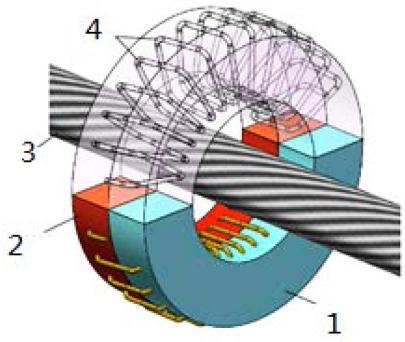

1-hard magnetic material; 2-soft magnetic material; 3-HVDC; 4-current-carrying coils

Fig. 3. (Color online) Entity Model of Magnetic Drive.

In order to improve the stability of the robot inspection during movement, the magnetic levitation system model of the inspection robot is designed to be rounded to facilitate nesting inside the overall structure of the robot, as shown in Fig. 2.

As is shown in Fig. 3, the magnetic drive system is also divided into upper and lower body parts. Current-carrying coils are wrapped in the upper body and the lower body. The processing technology is similar to the magnetic levitation system.

3. Realization Principle of the Magnetic Levitation System

3.1. Magnetic Levitation Principle Analysis and Model Design

According to the properties of the toroidal magnetic field determined by the DC current, the current-carrying coil is arranged in a rationally symmetric manner around the high-voltage conductor. As a result, the current-carrying coil is subjected to the work force in the magnetic field around the high-voltage line. The Ampere force is generally insignificant to overcome the gravity of the robot itself to suspend the robot on the high-voltage line. $\boldsymbol{L_2}$ $\boldsymbol{L_3}$, the long side of the current-carrying coil, is placed in a soft magnetic material due to the high permeability of soft magnetic materials. In contrast, $\boldsymbol{L_1}$ placed in a weak magnetic material (Air, etc.). By this, the Ampere force applied to the coil is in the upward direction, overcoming the weight of the robot and causing it to levitate. The magnetic levitation of the physical model is shown in Fig. 4.

To prevent the leakage of magnetic field, $\boldsymbol{L_2}$, the long

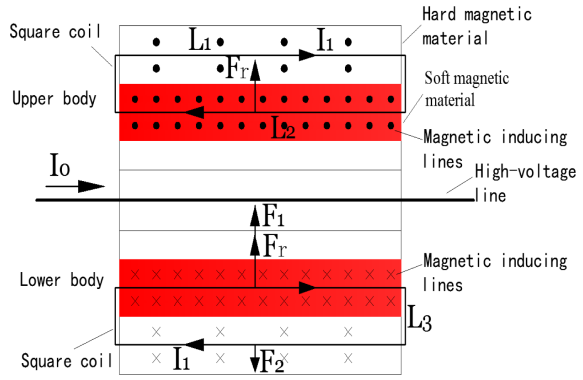

Fig. 4. (Color online) Magnetic levitation physical model.

side of the coil is seamlessly embedded in the soft magnetic material by 3D printing or sintering process. In order to reduce the difficulty in the manufacturing process of the magnetic suspension system, the long end of the coil L_2 is welded to the weak magnetic material. The magnetic suspension system is designed into the upper and lower body parts to meet the demands of opening and closing. The current-carrying coils are wrapped around the levitation system.

Since, the current carrying coil and the ring magnetic induction line are perpendicular to each other ($\theta = 90^{o}$), according to Ampere's law the Ampere force of the effective edge can be obtained as,

$$F = BIL \sin 90^{o} = BIL$$

where, B is the magnetic induction intensity; I is the current intensity. L is the wire length.

According to the analysis model of cross-section of magnetic suspension system of Fig. 5, the outer wire is in

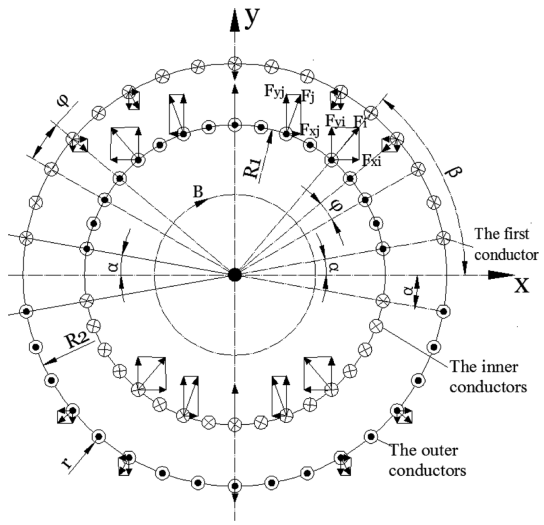

Fig. 5. Force Analysis of the Model Cross-section Coils.

a weak magnetic material (such as in the air), hence the strength of the magnetic field generated by the outer conductor can be expressed by Biot-Savart's law:

$$B_2 = \frac{\mu_0 I_0}{2\pi R_2} \tag{1}$$

where, I_0 is the high-voltage wire current; R_2 is the distance between the outer ring wire and the high-voltage line, or the radius of the circle of the outer wire.

The Ampere force of the single outer wire is:

$$F_2 = \frac{\mu_0 I_0 I_1 L_1}{2\pi R_2} \tag{2}$$

where, L_1 is the length of the long side of the wire in the field weakening material; I_1 is the current magnitude of the current-carrying coil.

As the inner ring wire is embedded seamlessly in the soft magnetic material, the magnetic field of the soft magnetic material enhances the magnetic field of the inner ring conductor. The magnetic field strength is given by:

$$B_1 = \frac{\mu_0 \mu_r I_0}{2\pi R_1} \tag{3}$$

where, μ_r is the relative permeability; R_1 is the distance between the inner conductor and the high-voltage axis, that is the radius of the circle of the inner conductor.

The Ampere force of the inner wire can be expressed as,

$$F_1 = \frac{\mu_0 \mu_r I_0 I_1 L_2}{2\pi R_1} \tag{4}$$

where: L_2 is the length of the long side of the wire in the soft magnetic material.

Assuming that the angle between the first wire and the X axis is α, the angle between the root wire and the X axis is β, the following condition is satisfied,

$$\beta = \alpha + \phi(i-1) \ \ (i = 1, 2, 3...n) \tag{5}$$

From Eq. (5), the components of the Ampere force in the Y axis direction can be obtained for a single coil,

$$F_y = (F_1 - F_2)\sin\left[\alpha + \phi(i-1)\right] \tag{6}$$

The winding of the upper and lower body of the magnetic levitation system is symmetrically arranged, so the levitation force of the entire system is,

$$\begin{aligned} F_{i2n} &= 2(F_{1y1} + F_{1y2} + \cdots + F_{1ym} + \cdots + F_{1yn}) \\ &\quad -2(F_{2y1} + F_{2y2} + \cdots + F_{2ym} + \cdots + F_{2yn}) \\ &= 2\sum_{i}^{n} (F_{1yi} - F_{2yi}) \end{aligned} \tag{7}$$

where, F_{1ym} is the force component of the Ampere force in the Y-axis direction of the m-th inner ring conductor placed in the soft magnetic material; F_{2ym} is the force component of the Ampere force in the Y-axis direction for the m-th outer ring conductor placed in the hard-magnetic material.

Substituting Eq. (7) into Eq. (6), we get the resultant force of the $2n$ current-carrying coils in the y-axis direction as,

$$\begin{aligned} F_{f2n} &= 2(F_1 - F_2)\{\sin[\alpha+\phi\times(1-1)]+\sin[\alpha+\phi\times(2-1)] \\ &\quad +\ldots+\sin[\alpha+\phi(m-1)]+\ldots+\sin[\alpha+\phi(n-1)]\} \\ &= 2\left(\frac{\mu_0\mu_r I_0 I_1 L_2}{2\pi R_1}-\frac{\mu_0 I_0 I_1 L_1}{2\pi R_2}\right)\times\sum_{i=1}^{n}\sin[\alpha+\phi\times(i-1)] \end{aligned} \tag{8}$$

Because the ampere force acting on the current-carrying conductor exceeds the axis of the high-voltage line, the torque acting on the inner and outer coils of the magnetic levitation system is zero.

$$\begin{aligned} M_o &= \sum_{i=1}^{n} F_{1i}\cdot 0 = 0 \\ M_i &= \sum_{i=1}^{n} F_{2i}\cdot 0 = 0 \end{aligned} \tag{9}$$

3.2. Magnetic Drive Principle Analysis and Model Design

The current-carrying coil is arranged in the magnetic field around the HVDC lines, and the Ampere force is used as the driving force of the direct traction robot. The magnetic drive physical model is shown in Fig. 6. L_5, the long side of the rectangular current carrying coil is placed in the soft magnetic material, and the corresponding long edge is placed in the hard magnetic material.

The extent of the magnetic field on each side of the coil of varies, so the Ampere force of the long side of the rectangular coil placed in the weak magnetic material is,

$$F_4 = \int_{R_4}^{R_3}\frac{\mu_0 I_0}{2\pi r} I_1 dr$$

where, R_3 and R_4 are the vertical distances between the HVDC transmission line and the upper and lower sides of the coil, respectively; I_0 is the high-voltage line current; I_1 is the coil current.

The other long side of the current carrying coil is placed in the soft magnetic material, and its strengthened magnetic induction B_3 is,

$$B_3 = \frac{\mu_0\mu_r I_0}{2\pi r} \tag{10}$$

The Ampere force of the long side F_3 is,

$$F_3 = \int_{R_4}^{R_3}\frac{\mu_0\mu_r I_0}{2\pi r} I_1 dr \tag{11}$$

As the magnetic drive system is composed of two symmetrical bodies, the winding coil is arranged symmetrically up and down with the high voltage line as the center line. The Ampere force of the short side of the rectangular coil of the upper body is cancelled by the Ampere force of the short side of the rectangular coil of the lower body. F_0, the resultant force of a single coil is,

$$F_0 = F_3 - F_4 \tag{12}$$

Without considering the coupling of the magnetic field and other cases, the total driving force of the magnetic drive system is,

$$F_{d2n} = 2nF_0 \tag{13}$$

where, n is the number of turns in the upper body (or lower body) winding coil.

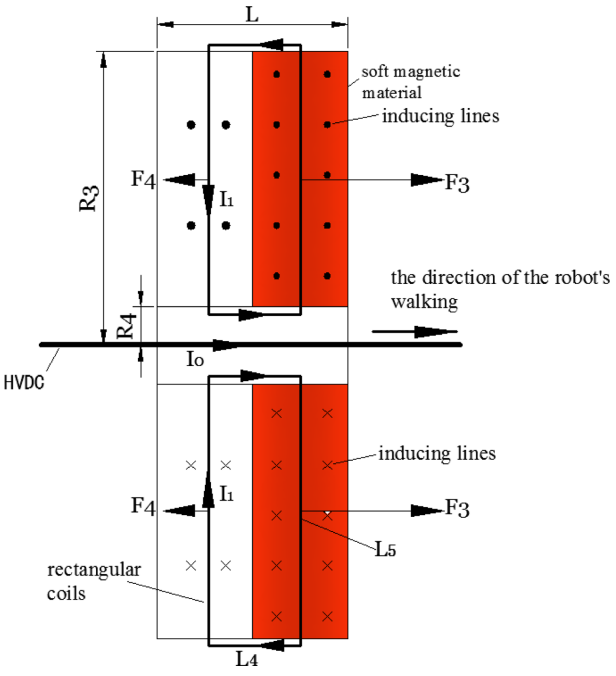

Fig. 6. (Color online) Physical Model of Magnetic Drive.

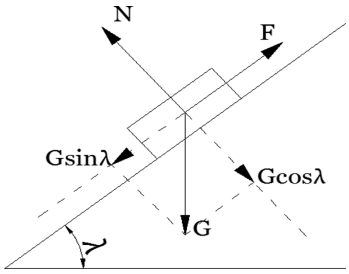

Fig. 7. Force Analysis of the Body in Slope Sections.

The robot travels on the high-voltage line by the guide wheel, and the rubbing friction is negligible. Considering the sag of the overhead high voltage line, the robot needs more traction in the uphill section with sagging. The line slope is shown in Fig. 7. To make the robot walk on the high voltage line, the following conditions must be satisfied,

$$F_{resul\tan t} \geq G\sin\lambda \tag{14}$$

4. Determination of Model Parameters

4.1. Relationship of Magnetic Levitation Model Length and Levitation Force

In order to obtain a large magnetic levitation force, the length of the effective side of the rectangular coil can be increased. However, an increase in the length of the long side of the coil, results in the robot becoming too heavy and not conducive for climbing. The relationship between the length of the model and the suspension force is established using a mathematical model.

The gravity ***G*** of the magnetic suspension system can be obtained as,

$$G = \rho_1\pi(R_2^2 - R_1^2)L_1 g \tag{15}$$

where ρ_1 is the average density of the magnetic suspension system model, ***g*** is the gravitational acceleration, g = 9.8 N/kg.

The condition for the levitation of the robot is,

$$F_{f2n} \geq G \tag{16}$$

$$2\left(\frac{\mu_0\mu_r I_1 I_2 L_3}{2\pi R_1} - \frac{\mu_0 I_0 I_1 L_1}{2\pi R_2}\right) \times \sum_{i=1}^{n} \sin[\alpha + \varphi\times(i-1)]$$

$$\geq \rho_1\pi(R_2^2 - R_1^2)L_1 g \quad (i = 1, 2, 3...n) \tag{17}$$

Considering, $L_1 = L_2$ in the magnetic levitation, Eq. (12) can be simplified as,

$$\left(\frac{\mu_0\mu_r I_0 I_1}{\pi R_1} - \frac{\mu_0 I_0 I_1}{\pi R_2}\right) \times \sum_{i=1}^{n} \sin[\alpha + \varphi\times(i-1)]$$

$$\geq \rho_1\pi(R_2^2 - R_1^2)g \tag{18}$$

It can be seen that the levitation force of the magnetic levitation system is proportional to the length of the magnetic suspension system, and the gravity of the magnetic suspension system is proportional to the length. However, under the condition of the levitation of the robot, the magnetic levitation of the system is independent of the length.

4.2. Magnetic Levitation Model Coil Turns Analysis

The magnetic levitation force can be enhanced by increasing the effective length of the long side of the coil or increasing the number of turns of the coils. In order to prevent the occurrence of leakage current in the coil of the magnetic material, the coil should not be made from enameled wire and should adopt the bare non-zero distance winding mode.

The magnetic levitation system is composed of upper and lower body, and the coils are arranged symmetrically. Considering the opening and closing action of the body, the coils are arranged in the range of α to $\pi-\alpha$ in the horizontal direction, as shown in Fig. 4. The arc length l_1 within the range of angles is,

$$l_1 = \frac{\pi - 2\alpha}{2\pi} R_1 \tag{19}$$

Assuming the inner ring coil zero distance winding distribution (in Fig. 8), and the center angle corresponding to the arc between the coil ***a*** and ***b***, the following can be obtained according to the trigonometric function relationship,

$$\delta_1 = 2\arcsin\frac{r}{R_1} \tag{20}$$

where, ***r*** is for the radius of cross-section of the coils.

The length of the arc which is through the center of the coil ***a*** and ***b*** is,

$$l_{ab} = \frac{\delta_1}{2\pi} R_1 \tag{21}$$

The ratio of the arc length between the upper and lower body of the magnetic levitation system to the effective arrangement of the coil and the arc length between ***a*** and ***b*** center is,

$$k_1 = \frac{2l_1}{l_{ab}} = \frac{2\pi - 4\alpha}{\delta_1} \tag{22}$$

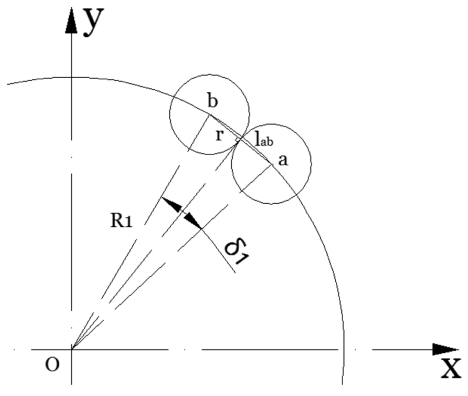

Fig. 8. Coils Zero-distance Distribution Parameter.

As can be seen from Eq. (22), when the imaginary coil is wound at zero distance, the upper and lower bodies can twist the coil k_1 turns at the greatest extent. Since the actual coil must guarantee non-zero distance when winding, the number of turns must be less than the k_1 turn when the coil is wound.

4.3. Relationship of Magnetic Drive Model Radius and Drive Force

In order to obtain larger magnetic driving force, the length of the long side of the rectangular coil can be increased. But the radius of the model increases correspondingly, leading an increase in the size of the robot. A mathematical model is used to establish the relationship between the radius of the model and the magnitude of the driving force, and the optimum range of the outer radius of the model.

The gravity G of the magnetically driven system is,

$$G = \rho_2 \pi (R_3^2 - R_4^2) Lg \tag{23}$$

where, ρ_2 is the average density of the magnetic drive system model.

The relationship between the outer radii of the magnetic drive system can be obtained as follows,

$$2n\left(\int_{R_4}^{R_3} \frac{\mu_0 \mu_r I_0}{2\pi r} I_1 dr - \int_{R_4}^{R_3} \frac{\mu_0 I_0}{2\pi r} I_1 dr \right) \geq \rho_2 \pi (R_3^2 - R_4^2) Lg \sin\lambda \ . \tag{24}$$

Equation (24) can be used to establish the following functions,

$$\begin{cases} f(R_3) = \dfrac{n\mu_0 I_0 I_1 (\mu_r - 1)}{\pi} \ln\left(\dfrac{R_3}{R_4}\right) \\ g(R_3) = \rho_2 \pi (R_3^2 - R_4^2) Lg \sin\lambda \end{cases} \tag{25}$$

The optimum range of the outer radius of the model is calculated as,

$$R_4 < R_3 \leq M(R_4) \tag{26}$$

where, $M(R_4)$ is the non-zero intersection abscissa of function $f(R_3)$ and $g(R_3)$.

According to Eq. (26) the magnetic drive system selection of the radius is not favored.

4.4. Magnetic Drive Model Coil Turns Analysis

In order to obtain higher driving force for the inspection robot, in addition to increasing the length of the long side of the coil, the number of turns of the coil can be increased.

The coil is appropriately arranged on the magnetic drive system, the angle between the body and the horizontal direction varies from ω to $\pi-\omega$. The coil in Fig. 9(a) is

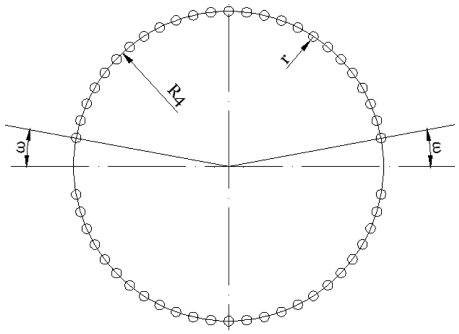

(a) coils distribution

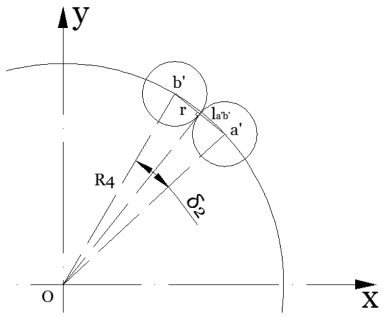

(b) Zero distance coils distribution

Fig. 9. Parameters of Coils Distribution.

appropriately distributed, and the arc length l_2 in the range of the angle is,

$$l_2 = \frac{\pi - 2\omega}{2\pi} R_4 \tag{27}$$

When the imaginary coil is wrapped at zero distance, as shown in Fig. 9(b), it is assumed that the center angle between the coil a and b is δ_2, which can be obtained according to the trigonometric relationship,

$$\delta_2 = 2 \arcsin \frac{r}{R_4} \tag{28}$$

where, r is the radius of the coil cross-section.

In Fig. 9(b), the length of the arc between the center of the coil a and center of b is,

$$l_{a'b'} = \frac{\delta_2}{2\pi} R_4$$

The ratio between the arc length of the coil arranged on the magnetic drive system and the arc length between the centers of coil a and b is,

$$k_2 = \frac{2l_2}{l_{a'b'}} = \frac{2\pi - 4\omega}{\delta_2} \tag{29}$$

Similarly, on the body in an imaginary, the actual coil winding to ensure non-zero distance, and the magnetic

drive system within a certain radius, so the number of turns winding must be less than k_2 turns.

5. Simulation Analysis and Theoretical Force Calculation

5.1. Establishment of Simulation Physical Model

Based on the design and optimization of the physical model, the parameters of the magnetic levitation system and the magnetic drive system should be instantiated in order to verify the validity of the model. The magnetic levitation system model and magnetic drive system model are established using COMSOL simulation software. Mn-Zn ferrite is used in the two systems. The relative permeability is as high as 15000. Considering the cost of material, the relative permeability is chosen to be 1000. As the current-carrying coil cannot withstand high current, $I = 10$ A is considered. Current carrying coil cross-sectional radius $\boldsymbol{r}$ is 0.0015 m.

In view of the magnetic levitation system, the magnetic field strength of the coil is greater close to the line surface. We take, $R_2 = 0.05$ m; In order to make the levitation system lighter, the extraction method is adopted with $L = 0.3$ m; In order to facilitate the opening and closing movements of the upper and lower bodies, $\alpha = 0^o$ is adopted. According to Eq. (22) the number of turns of the coil wound in the body must be less than 79. According to the characteristics of the solid model, a two-dimensional magnetic levitation simulation model is established according to the above parameters as shown in Fig. 10.

Aiming at the magnetic drive system, $L = 0.05$ m is

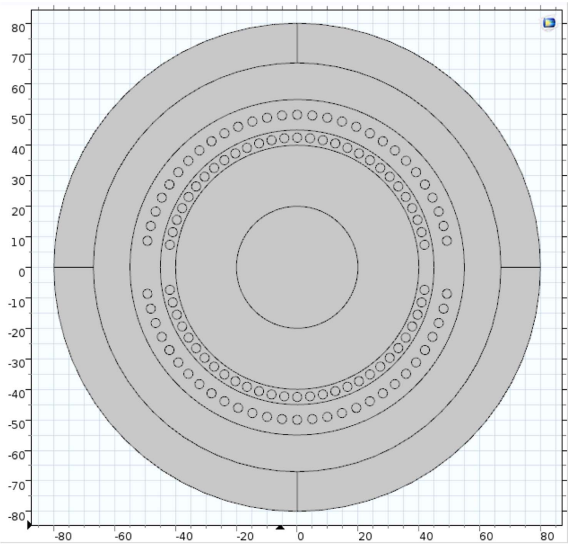

Fig. 10. (Color online) Simulation Model of Maglev Two-Dimensional.

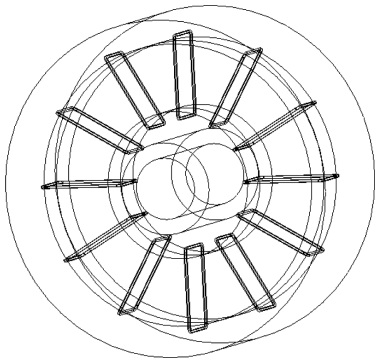

Fig. 11. Simulation Physics Model.

adopted to reduce the size of the robot. The maximum slope due to the sag of the overhead transmission line will not exceed 40 degrees, and hence $\beta = 40^o$. The magnetic drive system is composed of industrial iron, soft magnetic material, and is embedded in the coil. On account of these, the average density of the magnetic drive system for the current hypothesis is $\rho = 5 \times 10^3$ kg/m^3. Since the radius of the high-voltage cross-section is 0.02 m, the diameter of the small roller is 0.02 m, and the larger the Ampere force is, the larger the current is. According to the actual conditions, $R_4 = 0.048$ m. The optimum range of the outer radius of the model can be obtained by substituting the above values in Eq. (10):

$$0.049 \text{ m} < R_3 < 0.37 \text{ m} \tag{30}$$

In order to make the body lightweight, and small size, the following is considered, $R_3 = 0.092$ m and $\varphi = 10^o$ (Fig. 9(a)). According to Eq. (11) the body coils turns must be less than 89 turns. From the principle diagram and the optimum range of the outer radius of the model, the simulation physical model is set up as shown in Fig. 11. In order to facilitate the simulation, the winding coils in the solid model are equivalently simplified into single coil independent coils.

5.2. Simulation Analysis

Firstly, the material properties of the magnetic suspension system model are set, the physical field is selected as the magnetic field, the setting surface thickness is 0.3 m, the external current density of the high voltage line is $1000/(0.02 \times 0.02 \times \pi)$ A/m^2, the outer current density of the coil is $10/(0.0015 \times 0.0015 \times \pi)$ A/m^2, and all the coil calculations are included. The mesh partition is divided into three parts using the free-cut triangular mesh. The steady-state solver is used to solve the model.

Under the same model conditions, the coil current size is unchanged, and only the magnitude of the high voltage current is changed by simulation to 500 A, 1000 A, 1500

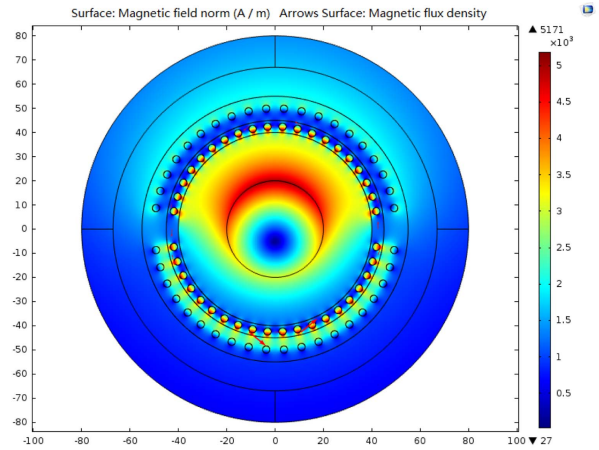

(a) $I_0 = 500A$

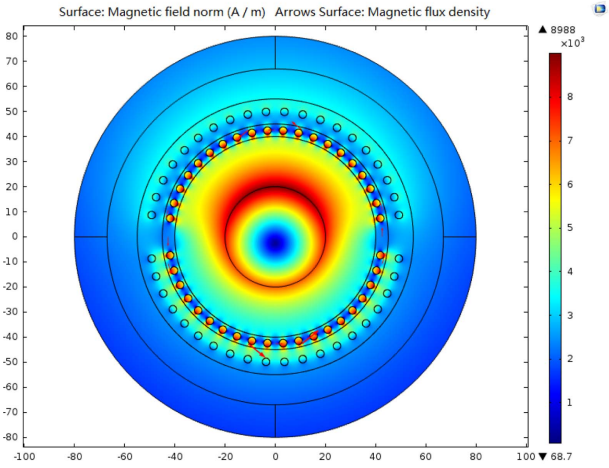

(b) $I_0 = 1000A$

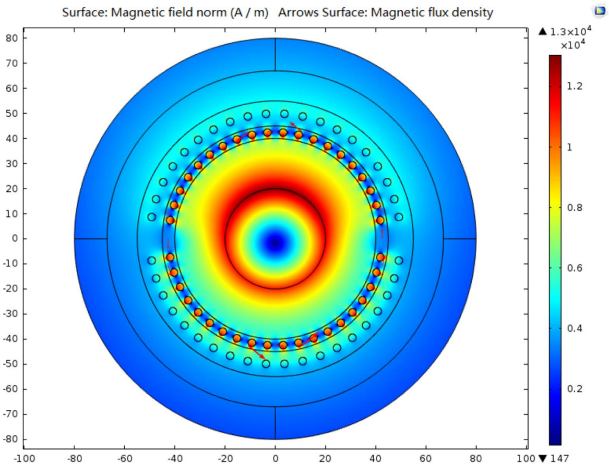

(c) $I_0 = 1500A$

Fig. 12. (Color online) Simulation of Different High-voltage Current Conditions.

A simulation shown in Fig. 12.

According to the two-dimensional simulation diagram,

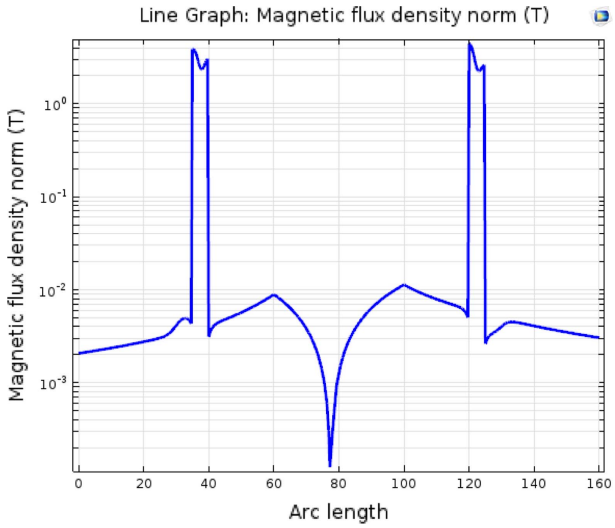

Fig. 13. (Color online) Curve Relation Curve of Arc Length Magnetic Flux Density.

the coil turns, coil current and other conditions are the same, with only the high voltage current increasing along with the surrounding magnetic field strength.

Based on the two-dimensional simulation model (Fig. 11) taking $x = 0$ as the two-dimensional line, simulation figure curve arc length and the magnetic flux density model are shown in Fig. 13.

The arc length is obtained to be around 80, which is close to the high-pressure line of two-dimensional model of the axis, magnetic flux density mode is minimal. When the two-dimensional section passes through the two current-carrying coil holes (i.e., in Fig. 13 shows the arc length value near 37.5 and 122.5 near), the magnetic flux density modes at the two locations are abrupt.

Maxwell's stress tensor can be expressed as a matrix:

$$\begin{aligned} T &= T^{(e)} + T^{(m)} \\ &= \varepsilon_0 \begin{bmatrix} E_x^2 - \dfrac{E^2}{2} & E_x E_y & E_x E_z \\ E_y E_x & E_y^2 - \dfrac{E^2}{2} & E_y E_z \\ E_z E_x & E_z E_y & E_z^2 - \dfrac{E^2}{2} \end{bmatrix} \\ &\quad + \frac{1}{u_0} \begin{bmatrix} B_x^2 - \dfrac{B^2}{2} & B_x B_y & B_x B_z \\ B_y B_x & B_y^2 - \dfrac{B^2}{2} & B_y B_z \\ B_z B_x & B_z B_y & B_z^2 - \dfrac{B^2}{2} \end{bmatrix} \end{aligned} \tag{30}$$

where, E_x, E_y and E_z represent the electric field com-

Table 1. Simulation results of Ampere force in the three-axis direction.

F/N	I_0 = 500 A	I_0 = 1000 A	I_0 = 1500 A
z	6.84×10^{-5}	1.31×10^{-4}	1.70×10^{-4}
x	–0.465	–1.048	–1.756
y	207.78	415.59	623.40

Note: under the same number of turns and different high voltage currents

ponents of the three directions of the surface element in x, y and z, respectively. B_x, B_y and B_z represent the magnetic component of the elements in the three directions, respectively. According to the integral of the surface element, the expression of the calculated force is,

$$F = \int_{\partial\Omega} nTds \tag{31}$$

Combining Eqs. (30) and (31), the magnetic levitation system with 40 turns is evaluated by software. In the case of high-voltage current of 500 A, 1000 A and 1500 A, the magnetic levitation system is obtained in ***x***, ***y*** and ***z*** direction. The magnitude of the Ampere force is shown in Table 1, where the Ampere force in the y direction is the levitation force of the robot (the negative data in Table 1 indicates that the Ampere force is opposite to the original direction).

For studying the change of the magnetic levitation force with the number of turns of the coil, the rule of the model coil is first analyzed (in Fig. 14). The coil at each point on the circumference of the Ampere force is not equal. Specifically, number 1 to 4 coil for the fixed point (the position is not fixed), and then each model gradually increases by 4 turns (up and down the body of the 2 turns). The upper and lower body coil and other center of the circle are evenly distributed. Different turns of the coil model in the high voltage current of 1000 A are simulated. Figure 15 (a) and (b) are the two-dimensional model of

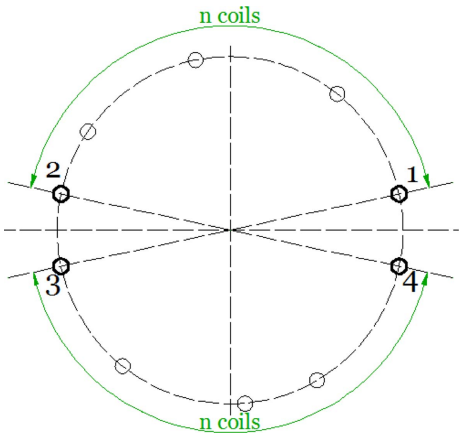

Fig. 14. (Color online) Coil Addition Distribution.

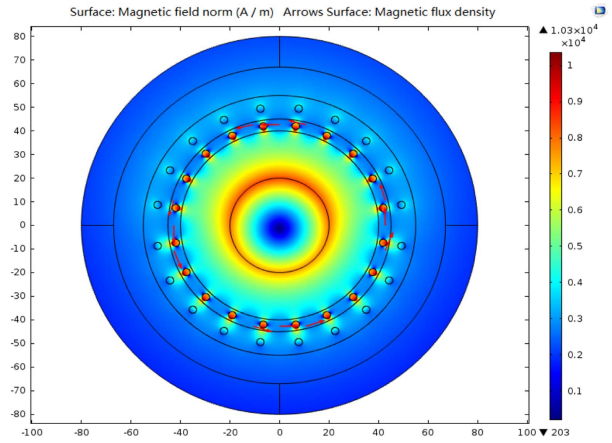

(a) 20 turns

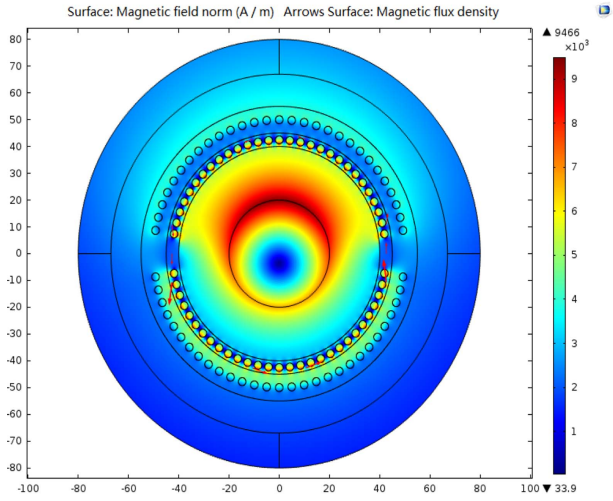

(b) 58 turns

Fig. 15. (Color online) Two-dimensional Model Simulation.

the magnetic levitation system with the number of turns of 20 and 58, respectively.

The following can be observed from the simulation diagram; from the distribution of the current density in the cross-section of the high voltage line, it is evident that the edge is larger than the center and the skin effect is obvious. The magnetic field around the coil embedded in the soft magnetic material in Fig. 15(a) is stronger than that in the hard-magnetic material. The magnetic field strength of the cross-section of the coil shows a strong radial magnetic field, while the two sides are weak; Fig. 15(b) shows the same analysis. When the number of turns in the coils increases, the magnetic flux density immediately above the high voltage line gradually increases, and the bottom of the magnetic flux density is gradually weakened. The direction of the magnetic induction line generated by the high voltage line and the direction of the

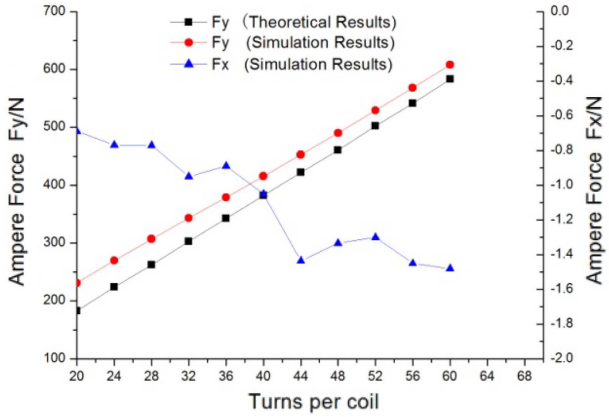

Fig. 16. (Color online) Comparison of Theoretical and Simulated Values.

magnetic induction line generated by the current carrying coil are determined by the right-hand rule. When the direction of the former coincides with the latter direction, the magnetic field strength is strengthened; when the direction of the former is opposite to the latter direction, it is weakened. When the number of turns is 58, the simulation results are:

$$\begin{aligned} F_{58y} &= 588.45N \\ F_{58x} &= -1.66N \\ F_{58z} &= 2.11\times 10^{-5}\ N \end{aligned} \tag{32}$$

The number of coils of the magnetic suspension system calculated by software are 20, 24, 28, ..., 56, 60. The size of the Ampere force in the x, y and z directions of the suspension system is F_x, F_y and F_z, where the y direction of the Ampere force F_y corresponds to the robot's levitation force. Draw the ampere size curve of the magnetic levitation system through the OriginPro software. The theoretical values and simulation values of the comparison are shown in Fig. 16. It can be seen from Fig. 16 that the simulated F_y is always larger than the theoretical value. With the increase of the number of turns, the theoretical value of F_y is closer to the simulation value. The simulation value of F_y increases with the number of turns. Since F_z is one millionth of F_y, it is not shown.

The physical field is selected for magnetic field. Coil type is numeric. The coil current is 10 A. Under the high voltage current of 500 A, 1000 A, 1500 A, three conditions of high-voltage line current density are set. According to the boundary conditions of magnetically insulated magnetic insulation interface, the current direction of the coil is set; automatic calculation of current and steady-state solution of the model is performed, as shown in Fig. 17 under three different high-voltage current coils for simulation with 12 turns.

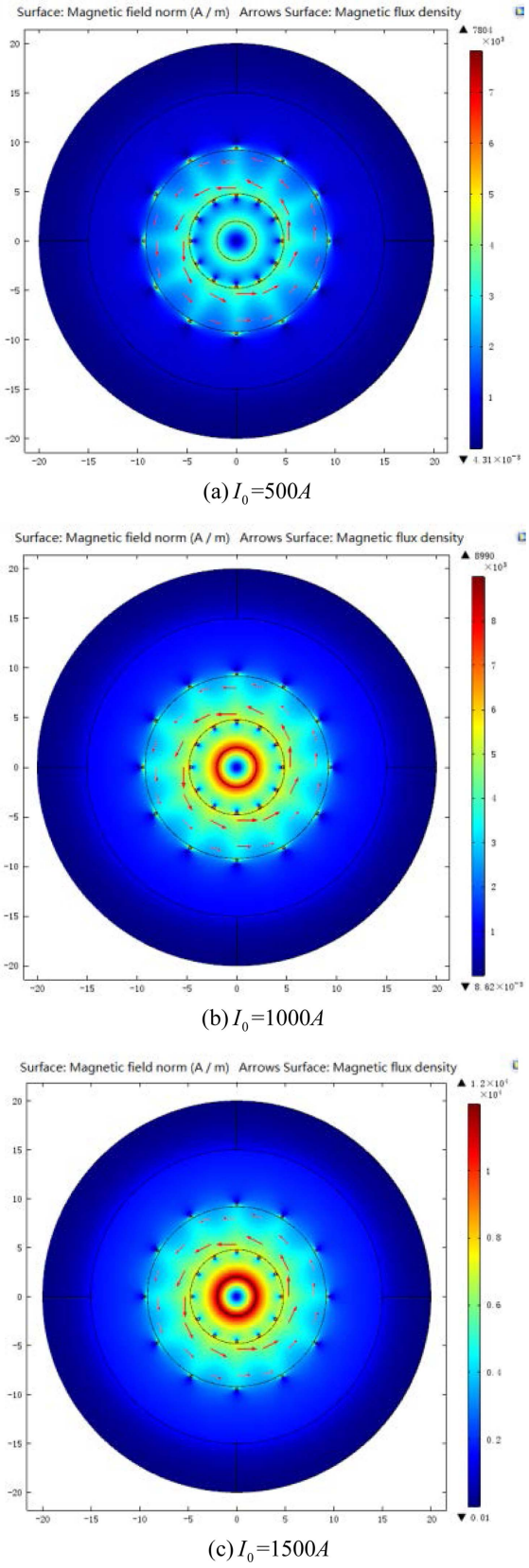

(a) I_0=500A

(b) I_0=1000A

(c) I_0=1500A

Fig. 17. (Color online) Same Model in Different Conditions of High-voltage Current Simulation Sectional Charts.

Table 2. Simulation results of ampere force magnitude in three axis direction of the same turn coil under different high-voltage currents.

F/N	I_0 = 500 A	I_0 = 1000 A	I_0 = 1500 A
z	–6.2929	–11.942	–17.604
x	8.8×10^{-3}	-3.2×10^{-2}	-7.5×10^{-2}
y	3.4×10^{-2}	8.7×10^{-2}	0.1643

According to the simulations, it can be seen that with the increase of the high voltage current, the magnetic field intensity increases continuously as long as the number of turns on the coil and the coil current are constant.

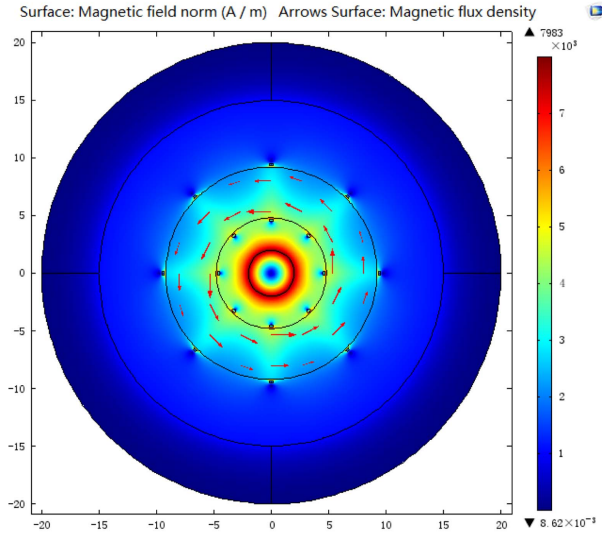

(a) 8 coil simulation cross sections

(b) 16 coil simulation cross sections

Fig. 18. (Color online) Sectional Charts of Model Simulation at the Same High-voltage Current.

Table 3. Simulation results of ampere force magnitude of turns of three coils in different axes.

F/N	1 turns	2 turns	4 turns
z	–0.948	–1.912	–3.853
x	-8.4×10^{-3}	2.5×10^{-4}	1.2×10^{-4}
y	2.8×10^{-2}	-6.2×10^{-2}	5.9×10^{-3}
F/N	8 turns	12 turns	16 turns
z	–7.813	–11.942	–16.229
x	3.3×10^{-2}	-3.2×10^{-2}	4.0×10^{-2}
y	2.0×10^{-2}	8.7×10^{-2}	7.3×10^{-3}

Combining Eq. (30) and (31), the magnetic force drive system with 12 turns coils is determined in the simulation. In the case of high voltage current of 500 A, 1000 A and 1500 A, the amber force is calculated in ***x***, ***y*** and ***z*** direction, where the amber force of the ***z*** direction is as the driving force of the robot.

The magnetic drive magnitude is calculated by changing the number of turns of the coil. Figure 18 shows the number of coils, where 8 and 16 are used to simulate the magnetic drive system model.

It can be seen from the simulation chart that the eight points on the outer diameter of the magnetic drive system in Fig. 18(a) are the cross-section of the coil, and the magnetic field strength on both sides of the coil cross section is stronger; Fig. 18(b) is analyzed on a similar basis. The magnetic field vector generated by the high-voltage line and the current carrying coil determined by the right-hand rule are consistent.

When the turns of the magnetic drive system are 1, 2, 4, 8, 12 and 16, the magnitude of the Ampere force of the coils in the three axis is calculated in the Table 3.

5.3. Theoretical Force Calculation

Without considering the magnetic field coupling and other factors, according to the required size of the magnetic levitation force, the number of turns needed to meet the coil under the conditions of the upper and lower body is taken to be $n = 29$; from Eq. (8) the theoretical levitation force of the model is:

$$F'_{f2n} = 2\left(\frac{\mu_0\mu_r I_0 I_1 L}{2\pi R_1} - \frac{\mu_0 I_0 I_1 L}{2\pi R_2}\right) \times \sum_{i=1}^{n} \sin\left[\alpha + \phi \times (i-1)\right] \approx 562N \tag{33}$$

The size of the Ampere force model supported by the magnetically driven model is:

$$F'_{d2n} = 2n\left(\int_{R_4}^{R_3} \frac{u_0 u_r I_0}{2\pi r} I_1 dr - \int_{R_4}^{R_3} \frac{u_0 I_0}{2\pi r} I_1 dr\right) \approx 78N \tag{34}$$

According to the coil turns analysis, the upper and lower body winding coil number is taken as $n = 30$.

6. Experiment

According to the aforementioned model parameters, the magnetic suspension device and the magnetic drive device are fabricated for experiments. The experimental equipment sets employed are: high current DC generator (range 0-1500 A), analog high-voltage wire, digital tension meter (range 0-500 N), magnetic suspension device (mass 3.5 kg, shown in Fig. 19). Strong magnetic material (magnetic conductivity of non-conductive) made of magnetic core. 60 coil holes drilled in the circumference of the magnetic core Peripheral lining is made of resin material The key parameters of the magnetic suspension device based on the previous theoretical calculations assume that: the relative permeability of soft magnetic materials is 1000; the inside diameter $R_0 = 0.045$ m, the outer diameter $R_2 = 0.055$ m; the coil current $I_0 = 10$ A (supplied by the battery). The simulation results in the previous section assume that the coil and the magnetically conductive material are in zero-distance contact, or the simulation is performed under the premise of no magnetic flux leakage. Therefore, in order to minimize the leakage flux, the coil is made of soft iron material. At the same time, after the coil passes through the hole, the powdery magnetic material of the same kind is mixed with the epoxy resin and then squeezed into the coil hole by pressure to fill the coil and the hole wall between the gap (to be clean and dry). In order to accurately measure the actual size of the magnetic levitation force, the experiment is placed in high-voltage wire level, high-voltage wire zero contact through the magnetic suspension device bore, the magnetic suspension device is directly linked to the tension meter hook, 50 kg weight.

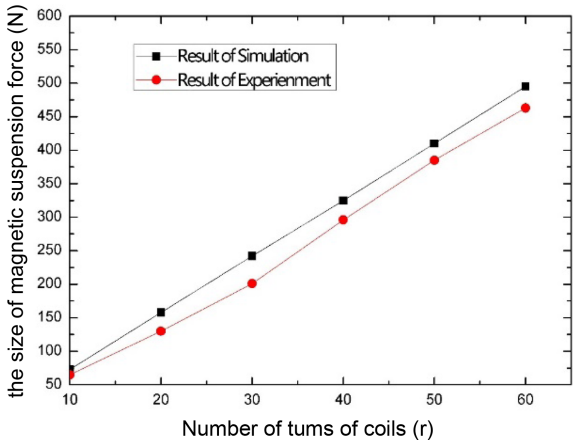

Fig. 20. (Color online) Comparison between experiment and simulation of magnetic suspension force.

(a) Current generator

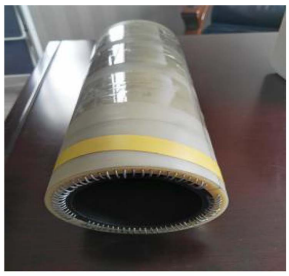

(b) Magnetic suspension device

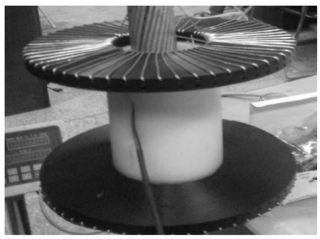

(c) Magnetic drive device

(d) Experimental setup

(e) Magnetic suspension measurement

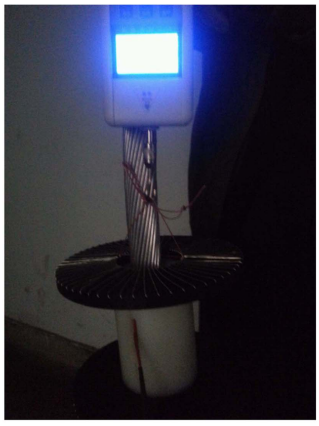

(f) Magnetic drive measurement

Fig. 19. (Color online) Experiment of Magnetic Suspension and Drive.

In the experiment, the winding method of the coil constantly changed, letting the coil pass 10, 20, 30, 40, 50, 60 holes in turn. The experiment is then then continued measuring the levitation force of the magnetic suspension system under different coil turns, and with the same condition. With the suspension force simulation value and the theoretical calculation of the value of the comparison, the results are shown in Fig. 20 (obtained in the chart experimental value has been subtracted by the magnetic suspension system weight).

In the case of different turns of the coil, the force of magnetic suspension increases with the number of turns of the coil, and the experimental measurements are very close to those of the ideal case. There is a slight difference between the experimental results and the simulation results in Fig. 20, which is mainly due to the local magnetic flux leakage caused by the local emergence of a small number of pores after the powder ferrite prepared by the epoxy resin is dried. The experiment proves that the proposed magnetic suspension model based on high-voltage DC magnetic field is accurate, and the magnetic suspension method is technically feasible.

7. Conclusion

Through the simulation analysis of the magnetic levitation system model and the magnetic drive system model, the following conclusions can be drawn:

(1) It can be seen that the theoretical value of magnetic levitation force is very close to the simulation value, which proves the validity of the magnetic levitation model proposed in this paper;

(2) It can be seen that the magnetic drive force F'_{d2n} calculated by theory is very close to the magnetic driving force F_{d60} obtained by the experiment, which proves the validity of the magnetic drive model proposed in this paper.

(3) Since the magnetic suspension system produces magnetic coupling, the magnetic induction line is biased and the component force is produced in the direction of x and y, the theoretical calculation value of the magnetic levitation force F'_{f2n} is not equal to the simulation value F_{58y};

(4) In the magnetic drive system when the coil number increases exponentially, the Ampere force is greater than the value and is not a linear relationship; when the current is changing the direction of current carrying coil, the driving force can be produced in the opposite direction allowing for slow-motion control of robot.

Acknowledgment

This work was supported by the National Natural Science Foundation of China (Grant No. 61375092), by the Hubei Science and Technology Support Program (Grant No. 2015BAA011).

References

[1] Zhu Xing-long, Zhou Ji-ping, Wang Hong-guang, and Fang Li-jin, Chinese Journal of Mechanical Engineering, **45**, 119 (2009).
[2] Zhang Yun-chu, Liang Zi-ze, Fu Si-yao, Tan Min, and Wu Gongping, Robot, **29**, 1 (2007).
[3] Zhou Feng-yu, Wu Ai-guo, Li Yi-bin, Wang Ji-dai, and Liang Zize, Automation of Electric Power Systems, **28**, 89 (2004).
[4] Pouliot, N. and Montambault, S., Geometric design of the LineScout, a teleported robot for power line inspection and maintenance [C]// Proceedings- ICRA 2008, Pasadena Conference center, Pasadena, CA, USA, 3970 (2008).
[5] Montambault, S. and Pouliot, N., Design and validation of a mobile robot for power line inspection and maintenance [C]// 6th International Conference on Field and Service Robotics-FSR2007, Chamonix, France; Springer: 495 (2008).
[6] Debenest, P., Expliner-robot for inspection of transmission lines[C]// Proceedings- ICRA 2008, Pasadena Conference Center, Pasadena, CA, USA: 3978 (2008).
[7] Wu Gong-ping, Cao Heng, Pi Yuan, and Fu Xing-wei, Engineering Journal of Wuhan University, **45**, 96 (2012).
[8] Wu Gong-ping, Xiao Xiao-hui, Xiao Hua, Dai Jin-chun, Bao Wu-jun, and Hu Jie, Automation of Electric Power Systems, **30**, 90 (2006).
[9] Wu Gong-ping, Dai Jin-chun, Guo Ying-long, Yu Jun-qing, and Yuan Wen-hua, Chinese Journal of Scientific Instrument, **20**, 571 (1999).
[10] Cheng Jiang-Feng, Rolling Stock, **41**, 13 (2003).
[11] Chen Qiang, Li Xiao-long, and Liu Shao-ke, Electric Drive for Locomotives, 52 (2014).
[12] Tang Su-ya, Micro-motor, **36**, 51 (2003).
[13] Mao Jun-hong, Luo Jun-hang, Jiang Qiang, and Xie You-bai, Journal of Xi'an Jiao tong University, **41**, 353 (2007).
[14] Chen Te-fang, Deng Jiang-ming, Tang Jian-xiang, and Cheng Shu, Control Engineering, **22**, 8 (2015).
[15] Hao Yang, Wang Zhang-yang, Yang Min, Xue Yong-feng, Li Xian-ting, and Xu Miao, Power System and Clean Energy, **28**, 49 (2012).